Center-of-mass motion as a sensitive convergence test for variational multimode quantum dynamics

Jayson G. Cosme,[1,*] Christoph Weiss,[2] and Joachim Brand[1]

[1]*New Zealand Institute for Advanced Study, Dodd-Walls Centre for Photonics and Quantum Technology, Centre for Theoretical Chemistry and Physics, Massey University, Private Bag 102904, North Shore, Auckland 0745, New Zealand*

[2]*Joint Quantum Centre (JQC) Durham–Newcastle, Department of Physics, Durham University, Durham DH1 3LE, United Kingdom*

(Received 27 October 2015; published 3 October 2016)

Multimode expansions in computational quantum dynamics promise convergence toward exact results upon increasing the number of modes. Convergence is difficult to ascertain in practice due to the unfavorable scaling of required resources for many-particle problems and therefore a simplified criterion based on a threshold value for the least occupied mode function is often used. Here we show how the separable quantum motion of the center of mass can be used to sensitively detect unconverged numerical multiparticle dynamics in harmonic potentials. Based on an experimentally relevant example of attractively interacting bosons in one dimension, we demonstrate that the simplified convergence criterion fails to assure qualitatively correct results. Furthermore, the numerical evidence for the creation of two-hump fragmented bright soliton-like states presented by A. I. Streltsov *et al.* [Phys. Rev. Lett. **100**, 130401 (2008)] is shown to be inconsistent with exact results. Implications for understanding dynamical fragmentation in attractive boson systems are briefly discussed.

DOI: 10.1103/PhysRevA.94.043603

I. INTRODUCTION

Recent advances in the field of ultracold atoms have made it possible to observe the quantum dynamics of few to many particles under unitary time evolution [1]. The opportunity to explain and predict novel effects motivates computational approaches, which face the challenge of vast complexity [2,3]. Variational multimode dynamics seeks to reduce the computational complexity by expanding the wave function with a small number M of optimized mode functions [4–7]. Specifically adapted for bosonic particles is the multiconfigurational time-dependent Hartree method for bosons (MCTDHB) [8]. It provides a hierarchy of approximations beyond the Hartree or Gross-Pitaevskii mean-field theory [9], to which it reduces for $M = 1$. The ability to represent fragmented Bose-Einstein condensates and correlated wave functions for $M > 1$ is the defining feature of the approach. While the limit of large M formally recovers the multiparticle Schrödinger equation, it is often impossible to verify convergence through increasing M due to prohibitive computational requirements. This motivates the search for independent convergence checks.

Here we test the convergence of MCTDHB simulations by exploiting the artificial coupling of the center-of-mass (c.m.) and relative motion in the truncated multimode expansion. In harmonic external potentials and homogeneous gauge fields, the c.m. dynamics of a many-particle system is independent of the particle interactions by the generalized Kohn's theorem [10,11]. Including time-dependent, anisotropic, rotating, or absent trapping potentials of any number of spatial dimensions, this result covers a wide range of experimentally relevant scenarios, where the exact quantum mechanical time evolution of the c.m. can be easily obtained. Since a convergent simulation is typically required to reproduce the exact c.m. dynamics, a comparison between both results serves as a sensitive convergence test.

An interesting scenario for quantum dynamics with ultracold atoms is provided by attractive bosons in narrowly confining elongated traps, where bright matter-wave solitons of 10^2 to 10^4 atoms have been observed [12–17]. Fragmentation of the Bose-Einstein condensate can be anticipated from theoretical arguments [18], even though experiments have been largely consistent with Gross-Pitaevskii ($M = 1$) theory. The tendency to form many-particle bound states [19], which are themselves well approximated by the Hartree approximation [20], further motivates the use of multimode expansions, and several MCTDHB-based studies have been published [21–23]. In this work we find a pathologically slow convergence of the MCTDHB expansion for untrapped or weakly trapped attractive bosons where the c.m. length scale becomes of the same order or larger than the typical length scale of relative motion. Specifically, we find that predictions for the dynamical creation of the two-humped, twofold fragmented states of attractive bosons named "fragmentons" in Ref. [21] were based on unconverged MCTDHB simulations and are inconsistent with the exact c.m. dynamics. We further find that previously proposed internal convergence checks of MCTDHB fail to reliably detect unconverged results, including the popular strategy of setting a threshold for the smallest eigenvalue of the single-particle density matrix to estimate the relevance of the least important mode [4,5,24].

II. MULTIMODE EXPANSION FOR ONE-DIMENSIONAL BOSONS

For definiteness, we consider the dynamics of N bosons of mass m in one dimension with the Hamiltonian

$$\hat{H} = \sum_{i=1}^{N} h(x_i,t) + g(t) \sum_{i<j} \delta(x_i - x_j) = \hat{H}_R + \hat{H}_r, \qquad (1)$$

where $h(x,t) = -\frac{\hbar^2}{2m}\frac{\partial^2}{\partial x^2} + \frac{1}{2}m\omega(t)^2x^2$, and $g < 0$ is the coupling parameter of attractive interactions [25]. Due to the harmonic trapping potential the problem is separable and the c.m. Hamiltonian $H_R = -\frac{\hbar^2}{2Nm}\frac{\partial^2}{\partial R^2} + \frac{1}{2}Nm\omega(t)^2R^2$ formally

*j.cosme@massey.ac.nz

defines a single-particle problem in the c.m. coordinate $R = N^{-1}\sum_i x_i$. The Hamiltonian of relative motion H_r depends only on the $N-1$ distances between particles and commutes with H_R. Thus the time evolution of any observables that are purely related to the c.m. coordinate is completely independent of the interaction strength. This is very useful for checking the convergence of multimode simulations.

The MCTDHB method is based on the variational ansatz for the quantum state

$$|\Psi(t)\rangle = \sum_{n_1,\ldots,n_M} C_{n_1,\ldots,n_M}(t) \prod_{k=1}^{M} \frac{1}{\sqrt{n_k!}} [\hat{b}_k^\dagger(t)]^{n_k} |\mathrm{vac}\rangle, \quad (2)$$

with $N = \sum_{k=1}^{M} n_k$ particles. Both the expansion coefficients and the single-particle functions $\phi_k(x,t) = \langle x|\hat{b}_k^\dagger(t)|\mathrm{vac}\rangle$ are time dependent and their evolution equations follow from a variational principle (for details see Ref. [8]). The main parameter determining the accuracy and computational effort of MCTDHB simulations is the number of single-particle modes M. The c.m. variance $\sigma_R^2 \equiv \langle (R - \langle R\rangle)^2\rangle$ can be obtained from (2) through the two-particle density $\rho^{(2)}(x,y) = \langle \hat{\psi}^\dagger(x)\hat{\psi}^\dagger(y)\hat{\psi}(x)\hat{\psi}(y)\rangle$ as [26]

$$\sigma_R^2(t) = \int \frac{x^2 + (N-1)xy}{N^2(N-1)} \rho^{(2)}(x,y;t)\, dxdy. \quad (3)$$

Since the multimode expansion (2) refers to single-particle quantities rather than the separated c.m. and relative coordinates, it does not trivially respect the separability. The simulated time evolution of the c.m. variance will thus be exact in two limits: when the multimode expansion (2) is fully converged or when particle interactions vanish ($g = 0$). In the latter case the MCTDHB time evolution reduces to uncoupled single-particle Schrödinger equations, which can be solved accurately within the chosen discretization scheme [8]. A simple convergence test is thus obtained by rerunning a given simulation with $g = 0$. If the interacting simulation is fully converged, the resulting time evolution of the c.m. must agree in both cases (see Appendix B for proof).

III. SIMULATING QUENCH DYNAMICS

As an example we consider the quantum time evolution of a bright soliton state following Ref. [21]. The initial state is prepared as a simple product state ($M = 1$) of $N = 1000$ bosons with $\phi_1(x,0) \propto \mathrm{sech}(x/\ell)$, where ℓ is a unit length scale, and the time evolution is simulated with MCTDHB in the absence of a trap [i.e. $\omega = 0$ in Eq. (1)] and with $gm\ell/\hbar^2 = -0.008$. The time evolution diagrams of the single-particle density with $M = 1$ and $M = 2$ shown in Figs. 1(a) and 1(b) are consistent with the previously published results (see Fig. 1, case III, in Ref. [21]). The c.m. variance shown in Fig. 1(d) deviates strongly from the exact time evolution and demonstrates that the MCTDHB results are unconverged.

Streltsov *et al.* [21] used the simulation result in Fig. 1(b) as evidence for the dynamical formation of two-hump fragmented states. They argued that the simulation corresponds to an interaction quench where the initial state, which is a Gross-Pitaevskii-level approximation to a bright matter wave soliton, is suddenly subjected to increased interactions. While a splitting into two equal-sized fragments or solitons

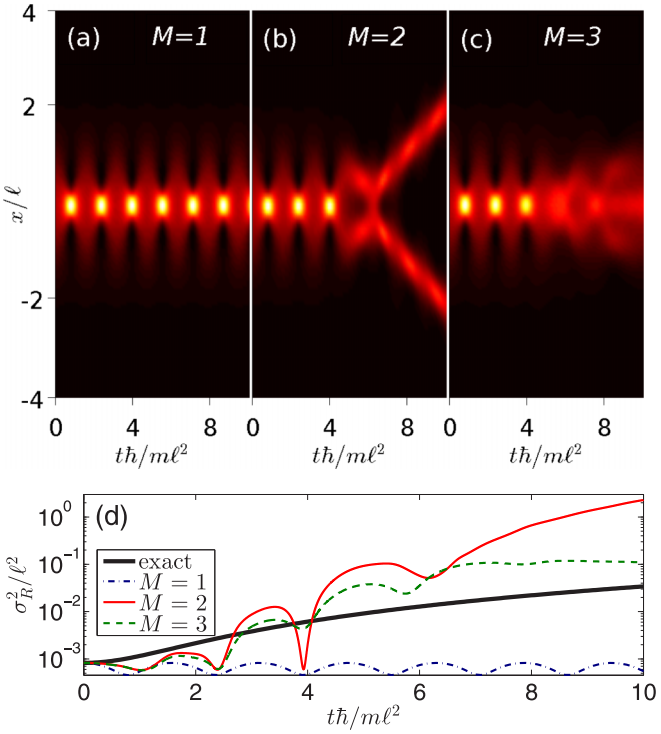

FIG. 1. Time evolution of $N = 1000$ attractive bosons prepared in a product initial state corresponding to a mean-field soliton following Ref. [21]. (a–c) Time evolution of the single-particle density $\langle \hat{\psi}^\dagger(x)\hat{\psi}(x)\rangle$ from MCTDHB simulations for different mode numbers. The $M = 2$ simulation (b) was used in Ref. [21] as evidence for the dynamical formation of two-humped fragmented quantum states called "fragmentons." (d) The time evolution of the c.m. variance is compared to the exact result (thick line) from a $g = 0$ simulation.

is energetically not possible in the Gross-Pitaevskii equation ($M = 1$), a fragmented Fock state of the form $|N/2, N/2\rangle$ with overlapping two-hump functions $\phi_{1/2}$ is energetically allowed and can be described within the multimode expansion (2) with $M = 2$ modes [21]. This argument is consistent with the splitting of the single-particle density into two rapidly parting fragments shown in Fig. 1(b), but the exact time evolution of the c.m. variance is not. The outward motion of the fragments starting shortly after $t = 6m\ell^2/\hbar$ goes in hand with a rapid increase in the c.m. variance as shown by the thin (red) line in Fig. 1(d), increasing to almost two orders of magnitude larger than the exact dynamics of σ_R^2 at $t = 10m\ell^2/\hbar$. This leads us to the conclusion that dynamical fragmentation cannot happen in just the way that was described in Ref. [21], but it leaves open the question whether other dynamical processes might favor the formation of "fragmentons." The $M = 3$ simulation [Figs. 1(c) and 1(d)], which was not available at the time of publication of [21], shows significant changes compared to the $M = 2$ case and further demonstrates that two modes are not sufficient to describe the exact quantum dynamics. Careful examination of the early-time dynamics of the c.m. variance in Fig. 1(d) reveals an interesting observation: MCTDHB consistently (for $M = 1,2,3$) predicts an initial decrease in the c.m. variance, while the exact σ_R^2 increases monotonically. This illustrates

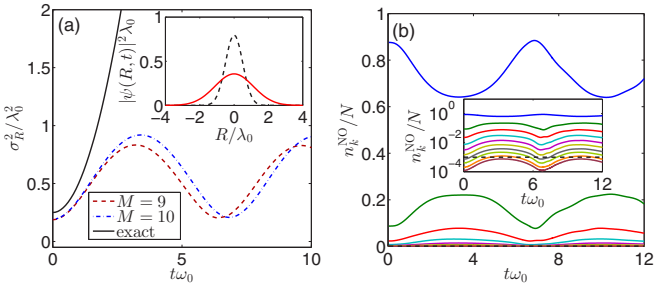

FIG. 2. Time evolution of $N = 2$ particles after sudden release from a harmonic trap; $gm\lambda_0/\hbar^2 = -3.16$. (a) Center-of-mass (c.m.) variance exact time evolution $\sigma_R^2 = \lambda_0^2(2N)^{-1}[1 + (\hbar t/m\lambda_0^2)^2]$ (solid line) and MCTDHB simulation with $M = 10$ modes (dashed line) showing unphysical breathing oscillations. Inset: c.m. wave function before ($t = 0$; dashed line) and after ($t\omega_0 = 2$; solid line) trap release. (b) Eigenvalues of the single-particle density matrix for the MCTDHB simulation. Inset: Semilogarithmic scale showing that the lowest occupancy is below the threshold value 10^{-3} for all times.

the artificial coupling of the c.m. with the contracting relative coordinates in MCTDHB. However, importantly, the graphs for $M = 2$ and 3 are on top of each other until $t \approx 1\, m\ell^2/\hbar$. Without the knowledge of the exact c.m. dynamics, judging from the observed succession of MCTDHB results under the assumption that the multimode expansion (2) is convergent, one would come to the erroneous conclusion that the observed contraction of the c.m. variance at early times was a reliable and converged result. The obvious discrepancy with the exact result implies that a conventional convergence check based on observing the absence of change while increasing the mode number M fails in this example. Many more modes would be required to converge the multimode expansion (2), which is unfeasible. For this reason it is particularly important to be able to solve the c.m. dynamics exactly in order to detect these artifacts of the simulation.

In order to better understand the convergence properties of MCTDHB for attractive bosons we consider a closely related, exactly solvable, and experimentally realizable scenario where two bosons are initially prepared in the ground state of a harmonic trap with frequency ω_0 and released from the trap at $t = 0$. Simulating the dynamics with up to $M = 10$ modes provides a wealth of internal information that can be used to assess the convergence properties of MCTDHB. Figure 2 shows the results of an unconverged MCTDHB simulation with $M = 10$ modes.

IV. NATURAL OCCUPANCY CRITERION

The relevance of mode functions in the MCTDHB expansion is assessed by examining the eigenvalues n_k^{NO} of the single-particle density matrix, also known as natural occupancies, from $\langle\hat{\psi}^\dagger(x)\hat{\psi}(y)\rangle = \sum_{k=1}^{M} n_k^{NO}\varphi_k^*(x)\varphi_k(y)$, where $\sum_k n_k^{NO} = N$ and eigenvalues are ordered by size $n_1^{NO} \geqslant \cdots \geqslant n_M^{NO} \geqslant 0$. A rapidly decreasing sequence of eigenvalues in the exact single-particle density matrix is expected to signal convergence of the multimode expansion (2) [4]. Since exact results are usually not available, instead it has become popular to draw conclusions from the natural populations obtained from the variational MCTDHB simulation. A commonly used criterion assumes that the simulation is converged if the smallest relative population lies below a threshold value [27], and recently $n_M^{NO}/N < 10^{-3}$ has been used for ultracold-atom experiments [24,28–30] (10^{-2} in Ref. [31]). Recently, an alternative convergence check has been proposed where the truncation error during time evolution is estimated directly, but the scheme has not been implemented yet [32].

The results shown in Fig. 2 provide an example where the threshold criterion fails, while comparison of the c.m. dynamics with exact results clearly shows that the simulation is not converged. Beyond the possibility that simply a smaller threshold value may need to be set, we argue that the logic behind the threshold criterion is flawed because it ignores the possibility that (a) a large number of natural orbitals with very low occupancies can still make an important sum contribution to the density matrix, (b) the natural occupancy of the Mth mode may be underestimated by the variational approach, and (c) the nonlinear evolution equations of MCTDHB may amplify small inaccuracies in the fractional occupancies into large deviations of observables at later times. While good-natured examples were reported in the literature [33,34] where these problems do not arise, all three possibilities play a role in the breakdown of the criterion for attractive bosons. Specifically, the variational MCTDHB calculation of the trapped ground state (initial state in Fig. 2) yields the smallest natural occupancy, $n_{10}^{NO}/N = 1.2 \times 10^{-4}$ ($M = 10$), compared to the almost four times larger exact value of $n_{10}^{NO}/N = 4.5 \times 10^{-4}$ (exact), supporting concern (b). It validates point (a) that the cumulative contribution of natural orbitals beyond the 10 highest occupied, $1 - N^{-1}\sum_{i=1}^{10} n_i^{NO} = 1.4 \times 10^{-3}$ (exact), is an order of magnitude larger than the MCTDHB value for the 10th natural occupancy, confirming that the latter is a poor estimate for the former. Even though these numbers are several orders of magnitude smaller than unity and a reasonably faithful representation of the true quantum state might be expected, a 23% deviation of the c.m. variance from the exact value indicates a poorly converged result instead. Finally, rerunning the MCTDHB simulation with a slightly modified initial state (optimized to $M = 9$ modes) we indeed find a sensitive dependence on initial conditions as anticipated in point (c), where a change in the breathing frequency and amplitude will lead to completely different values of σ_R^2 after a few periods.

V. ROLE OF THE PARTICLE NUMBER

It is instructive to consider the convergence properties of MCTDHB in dependence of the available parameters. In contrast to the repulsive Bose gas, which has a dimensionless interaction parameter [35], the interaction strength scales out for untrapped attractive bosons and the only remaining dimensionless parameter is the particle number N [19]. A second dimensionless parameter is available in a harmonic trap by comparing relevant length scales. The ratio σ_R/σ_{sol} allows for a meaningful comparison of results between varying particle numbers and is thus used for comparing ground-state calculations of attractive bosons in Figs. 3 and 4. Here, $\sigma_R^2 = \lambda_0^2/(2N)$ is the ground state c.m. variance in the harmonic trap and $\sigma_{sol}^2 = \hbar^4\pi^2/[3g^2m^2(N-1)^2]$ is the variance of the

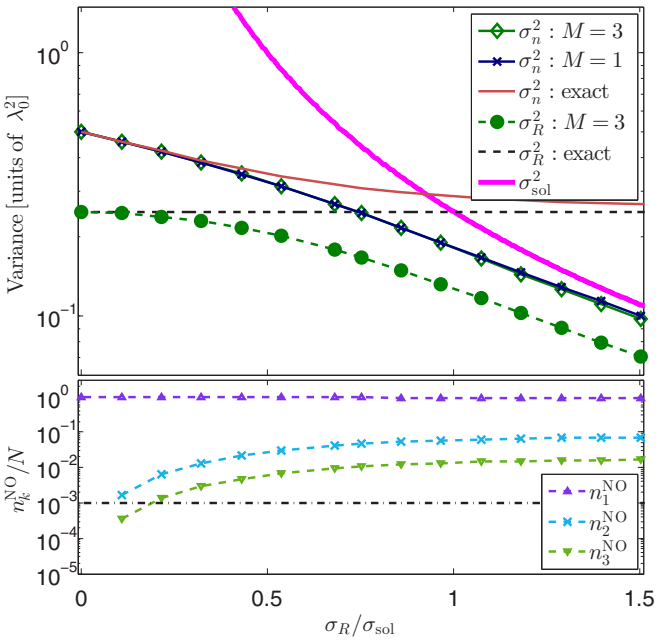

FIG. 3. Ground-state properties of harmonically trapped attractive bosons in one dimension for $N = 2$ particles as a function of the length-scale ratio $\sigma_R/\sigma_{\rm sol}$. Top panel: c.m. variance σ_R^2 and variance of the single-particle density σ_n^2 from exact and simulated MCTDHB results. Bottom: For comparison also the soliton variance $\sigma_{\rm sol}^2$ is shown. This relative motion length scale is clearly seen to influence the variational $M = 3$ result in the limit of a weak trapping potential.

soliton particle density $\propto \mathrm{sech}^2(\pi x/[2\sqrt{3}\sigma_{\rm sol}])$ obtained for the untrapped ground state with $M = 1$ [18], a characteristic length scale determined by particle interactions.

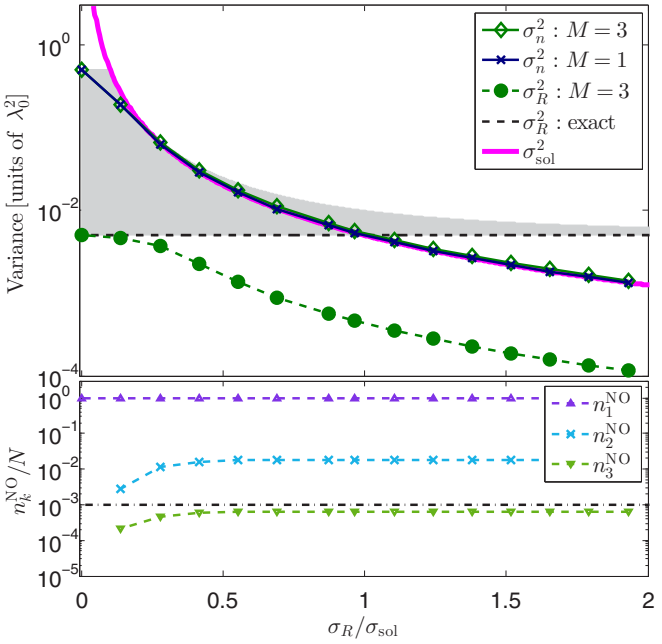

FIG. 4. Same as Fig. 3, with $N = 100$ bosons. The shaded region depicts the known limits for σ_n^2: $\sigma_R^2 \leqslant \sigma_n^2 \lessapprox \sigma_R^2 + \sigma_{\rm sol}^2$ (see Appendix E for proof).

The MCTDHB results for the variance of the single-particle density σ_n^2 and c.m. variance σ_R^2 in Figs. 3 and 4 show a good agreement with exact results only for $\sigma_R/\sigma_{\rm sol} \ll 1$, which is a weakly interacting or strong-trap limit where the harmonic potential dominates all length scales of the quantum state. As soon as the interacting length scale $\sigma_{\rm sol}$ becomes comparable to or smaller than the c.m. length scale, significant deviations from exact results occur for the numerically obtained σ_n^2 and σ_R^2. In the weak-trap regime $\sigma_R \gg \sigma_{\rm sol}$, the deviation can become arbitrarily large.

So could the failure of the MCTDHB approximation be detected by internal criteria, i.e., without comparison to exact results? This appears possible for $N = 2$ particles, where the threshold of 10^{-3} for the lowest occupancy would signal unconverged results for $\sigma_R/\sigma_{\rm sol} \gtrsim 0.2$. Inspecting the sequence of numerical results with increasing M further indicates that convergence is very slow (see Appendix D). The situation is far worse with $N = 100$ particles, where increasing M further may not be an option due to limited computational resources [36]. Analysis of the natural occpancies provides the consistent picture of an almost-pure Bose-Einstein condensate, with the least occupancy well below the threshold. Further, the main observable σ_n^2 displays little variation between $M = 1$ and $M = 3$ on the scale of Fig. 4 and clearly shows the same trend as a function of $\sigma_R/\sigma_{\rm sol}$. We are thus led to the conclusion that the detection of spurious results from MCTDHB is much more difficult and may even be impossible without exact results to compare with, for particle numbers of the order of 100 or larger.

VI. DISCUSSION AND CONCLUSIONS

Why is MCTDHB unable to capture the physics of the weak-trap regime, while the Hartree approximation ($M = 1$) is known to reproduce the exact, untrapped ground-state energy to leading order for large N [20], and previous work has found MCTDHB to converge nicely at large N [34]? The Hartree approximation fails to describe the delocalization of the c.m. in the untrapped limit [18] because the variational principle, conditioned to minimize the total energy, finds the best compromise in localizing the single available mode function $\phi_1(x)$. When a finite number $M > 1$ is used in the multimode expansion, it is still energetically advantageous to localize the mode functions. Indeed, an infinite number of mode functions is needed to represent a state with delocalized c.m. but bound relative motion (see Appendix D).

In conclusion, we have demonstrated how easily obtainable, accurate results for the c.m. variance were useful in detecting unconverged results and in demonstrating the failure of several popular internal convergence checks of MCTDHB. The possible dynamical creation of "fragmentons" is reopened for discussion, as numerical evidence in Ref. [21] turned out to be spurious. Our findings call for a systematic reevaluation of the available convergence criteria for numerical quantum dynamics and what is required to claim "numerically exact" results [24,31,37–39]. The comparison of c.m. dynamics with independent, exact results may be useful for other numerical methods of quantum dynamics and is available in any spatial dimensions and for any particle statistics as long as external potentials are at most harmonic.

ACKNOWLEDGMENTS

The data presented in this paper will be available online [40]. We thank L. D. Carr, B. Gertjerenken, M. F. Andersen, and W. P. Reinhardt for discussions and U. Fischer for pointing out Ref. [32]. This work was supported by the Marsden fund of New Zealand (Contract No. UOO1320) and the Engineering and Physical Sciences Research Council United Kingdom (Grant No. EP/L010844/1).

APPENDIX A: DETAILS OF NUMERICAL SIMULATIONS

Numerical simulations were performed with the open-source QiwiB implementation of the MCTDHB [41], using standard Runge Kutta time evolution and representing spatial derivatives with five-point stencil finite differences. For the $N = 2$ ground-state results in Figs. 3 and 4, we have performed simulations on a 1400-point equidistant grid with different values of the coupling constant g using $L = 30\lambda_0$ as the computational box length for $gm\lambda_0/\hbar^2 \geqslant -0.7794$ and $L = 14\lambda_0$ for stronger interactions, while for $N = 100$, we have used a 2000-point equidistant grid with $L = 30\lambda_0$ for $gm\lambda_0/\hbar^2 \geqslant -0.0714$ and $L = 10\lambda_0$ for stronger interactions. For the time evolution of the c.m. variance, we have used a 600-point equidistant grid with $L = 25\lambda_0$ for both $M = 9$ and $M = 10$ simulations. We have assured ourselves that the results are converged with respect to changes in these parameters and those of time and space discretization. In addition, we have compared the QiwiB results against an independent implementation of MCTDHB [42], which produced identical results at the reported accuracy. The simulations of the quench dynamics are performed in two steps: (i) relaxation to the ground state of the harmonic trap and (ii) time propagation after turning off the trap.

APPENDIX B: INTERACTION DEPENDENCE OF THE CENTER-OF-MASS VARIANCE

It follows from very general principles that observables linked only to the c.m. wave function are independent of the interaction strength for at most harmonic potentials or constant gauge fields. Here we demonstrate this explicitly for the c.m. variance and a many-particle system governed by the Hamiltonian in Eq. (1). For this purpose we write an arbitrary initial quantum state as

$$|\Psi_0\rangle = \sum_{\mu,\nu} c_{\mu\nu}|\chi_\mu\rangle|\Phi_\nu\rangle, \tag{B1}$$

where $\{|\chi_\mu\rangle\}$ is a complete basis set which depends only on the c.m. and $\{|\Phi_\nu\rangle\}$ is a complete basis set which depends on the $N-1$ relative motion degrees of freedom. We further write the time evolution of the many-body wave function as ($\hbar = 1$)

$$|\Psi(t)\rangle = e^{-i(\hat{H}_R+\hat{H}_r)t}|\Psi_0\rangle. \tag{B2}$$

In Eq. (B2), the total Hamiltonian was written as $\hat{H} = \hat{H}_R + \hat{H}_r$, where $\hat{H}_R$ is the c.m. Hamiltonian and the remaining terms, including the interaction-dependent operators, form $\hat{H}_r$. Then we can explicitly write

$$\begin{aligned}|\Psi(t)\rangle &= e^{-i(\hat{H}_R+\hat{H}_r)t}\sum_{\mu,\nu} c_{\mu\nu}|\chi_\mu\rangle|\Phi_\nu\rangle \\ &= \sum_{\mu,\nu} c_{\mu\nu}\left(e^{-i\hat{H}_R t}|\chi_\mu\rangle\right)e^{-i\hat{H}_r t}|\Phi_\nu\rangle.\end{aligned} \tag{B3}$$

The dynamics of the second moment of the c.m. wave function is obtained as

$$\begin{aligned}&\langle\Psi(t)|\hat{R}^2|\Psi(t)\rangle \\ &= \sum_{\mu',\nu'}\sum_{\mu,\nu} c^*_{\mu'\nu'}c_{\mu\nu}\langle\chi_{\mu'}|e^{i\hat{H}_R t}\hat{R}^2 e^{-i\hat{H}_R t}|\chi_\mu\rangle \\ &\quad\times(\langle\Phi_{\nu'}|e^{i(\hat{H}_r-\hat{H}_r)t}|\Phi_\nu\rangle) \\ &= \sum_{\mu',\mu,\nu} c^*_{\mu'\nu}c_{\mu\nu}(\langle\chi_{\mu'}|e^{i\hat{H}_R t}\hat{R}^2 e^{-i\hat{H}_R t}|\chi_\mu\rangle).\end{aligned} \tag{B4}$$

From the last line in Eq. (B4) it can be seen that the result is independent of the interaction strength during the time evolution. The time evolution of the c.m. variance thus depends only on the initial state (through the expansion coefficients $c_{\mu\nu}$) and the external potential through the c.m. Hamiltonian $\hat{H}_R$. This fact can be used as a sanity check for MCTDHB simulations, which, if fully converged, should produce the same time evolution for the c.m. variance for different values of the interaction strength.

APPENDIX C: EXACT SOLUTION OF THE TWO-PARTICLE PROBLEM

The ground state of $N = 2$ particles in a time-independent harmonic trap with frequency ω_0 is described by a product of the center-of-mass and relative motion wave functions: $\Psi(R,r) = \psi_0(R)\phi_0(r)$. The analytical form of the c.m. wave function is

$$\psi_0(R) = \left(\frac{2m\omega_0}{\pi\hbar}\right)^{1/4} e^{-m\omega_0 R^2/\hbar}, \tag{C1}$$

where $R = (x_1 + x_2)/2$. On the other hand, the relative motion wave function with the normalization constant A and harmonic oscillator length scale, $\lambda_0 = \sqrt{\hbar/m\omega_0}$, can be obtained as

$$\phi_0(r) = Ae^{-r^2/4\lambda_0^2}U\left(-\frac{\nu}{2},\frac{1}{2},\frac{r^2}{2\lambda_0^2}\right), \tag{C2}$$

where $r = (x_2 - x_1)$ is the relative coordinate, $U(a,b,x)$ is the confluent hypergeometric function of the second kind, and ν comes from the discontinuity in the first derivative due to the delta interaction [43]. Explicitly, ν is calculated by solving the transcendental equation

$$\nu = \frac{gm\lambda_0}{\hbar^2\sqrt{2}}\frac{\Gamma(1-\nu/2)}{\Gamma(1/2-\nu/2)}. \tag{C3}$$

The ground-state energy is given by

$$\begin{aligned}E_0^{2,\text{exact}} &= E_{\text{rel}} + E_{\text{c.m.}} \\ &= \hbar\omega_0\left(\nu+\frac{1}{2}\right) + \frac{\hbar\omega_0}{2} = \hbar\omega_0(\nu+1),\end{aligned} \tag{C4}$$

and the exact results for the natural occupancy are obtained by numerically diagonalizing the single-particle density matrix

$$\langle\hat{\psi}^\dagger(x)\hat{\psi}(y)\rangle = 2\int dz\Psi^*(x,z,t=0)\Psi(y,z,t=0)$$
$$= 2\int dz\psi_0^*((x+z)/2)\phi_0^*(x-z)$$
$$\times\psi_0((y+z)/2)\phi_0(y-z). \quad \text{(C5)}$$

After turning off the trap, the Gaussian c.m. wave function expands. In particular, the time evolution of the c.m. wave function represents the textbook example of Gaussian wave propagation [44]:

$$\psi(R,t) \propto \left(1+i\frac{\hbar t}{m\lambda_0^2}\right)^{-1/2}$$
$$\times\exp\left(-\frac{R^2}{\lambda_0^2\left[1+i\hbar t/\left(m\lambda_0^2\right)\right]}\right). \quad \text{(C6)}$$

The c.m. wave function spreads, leading to a variance increasing quadratically in time:

$$\sigma_R^2(t) = \frac{\lambda_0^2}{4}\left[1+\left(\frac{\hbar t}{m\lambda_0^2}\right)^2\right]. \quad \text{(C7)}$$

The relative motion after trap release, on the other hand, is dominated by the bound state of the attractive δ interactions. Indeed, since the δ function has exactly one bound state, the relative motion wave function near the origin will approach this bound state in the long-time limit and possible other contributions from the scattering state will disperse. The initial relative motion wave function can be expressed in terms of the bound state and scattering states: $\phi_0(r) = c_b\phi_{BS}(r) + \int dke^{ikr}c_k$, where the bound state is $\phi_{BS}(r) = \sqrt{\frac{m|g|}{2\hbar^2}}\exp(\frac{-m|g||r|}{2\hbar^2})$. Then the expected variance of the relative motion wave function in the long-time limit must be $\sigma_r^2 \geqslant \sigma_{BS}^2 = \int drr^2|\phi_{BS}(r)|^2 = 2\hbar^4/m^2g^2$.

APPENDIX D: MCTDHB SIMULATIONS WITH $N = 2$ PARTICLES

In the text we have demonstrated the ambiguity of studying the eigenvalues of the single-particle density matrix, the natural occupancies, for a specific MCTDHB simulation. For $N = 2$ particles we are able to vary the number of modes M over a good range, which permits a conventional study of convergence with respect to mode number. It is further possible to analyze the shape of the two-particle wave function in the MCTDHB approximation, which sheds some light on the unphysical coupling of relative and c.m. motion in the truncated multimode expansion.

1. Convergence of MCTDHB results with increasing M

We test the convergence by checking whether relevant quantities, e.g., the variational ground-state energy, remain unchanged as the number of modes M is increased. The results in Table I still vary at the level of several percent between $M = 8$ and $M = 10$ and thus indicate, correctly, that the MCTDHB expansion converges very slowly and is not yet fully converged with 10 modes. While this way of testing convergence is reliable and has produced the correct answer, varying M from 1 to 10 modes is a luxury that can only be afforded for small particle numbers N. In simulations with hundreds to thousands of particles (e.g., [21,23,45]), the options for choosing M are severely limited due to the unfavorable scaling of numerical effort when both N and M are large.

TABLE I. Ground-state energy E and the two largest natural occupancies (NOs) from MCTDHB calculations of $N = 2$ trapped bosons.

	$\tilde{g} = -3.1623$			$\tilde{g} = -2$		
M	$E/\hbar\omega_0$	n_0^{NO}/N	n_1^{NO}/N	$E/\hbar\omega_0$	n_0^{NO}/N	n_1^{NO}/N
1	−0.5787	1	0	−0.0915	1	0
3	−1.1451	0.9342	0.0536	−0.1356	0.9613	0.0316
5	−1.3817	0.9062	0.0701	−0.2244	0.9483	0.0392
8	−1.5546	0.8846	0.0825	−0.2788	0.9387	0.0451
10	−1.6213	0.8761	0.0872	−0.3005	0.9355	0.0470
Exact	−1.9527	0.8251	0.1142	−0.3993	0.9202	0.0563

We have also considered how the dependence of the c.m. variance of the trapped ground state on the interaction strength g changes for different numbers of modes M. For brevity, we introduce the dimensionless interaction parameter where $\tilde{g} = gm\lambda_0/\hbar^2$. For $N = 2$, this coupling constant is related to the ratio between relevant length scales via $\tilde{g} = -0.55\sigma_R/\sigma_{sol}$, where the prefactor changes with N. Figure 5 compares the c.m. variance from MCTDHB calculations with the exact result $\sigma_R^2 = \lambda_0^2/4$ from Eq. (2) in the text. It is apparent that the MCTDHB results deviate severely from the exact values

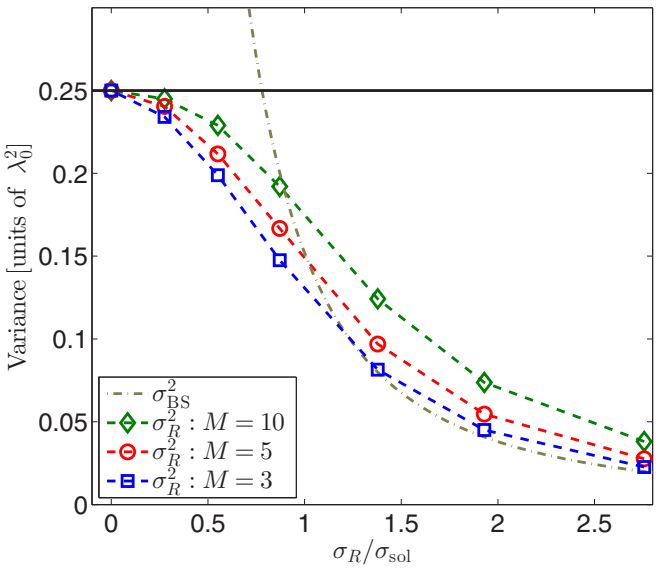

FIG. 5. Center-of-mass (c.m.) variance for the trapped ground state for $N = 2$ as a function of the length-scale ratio σ_R/σ_{sol} from MCTDHB simulations for different values of M (symbols). The solid horizontal line denotes the exact ground-state c.m. variance $\sigma_R^2 = \lambda_0^2/4$. For comparison, the dash-dotted line shows the exact relative-coordinate variance σ_{BS}^2 of the two-particle bound state.

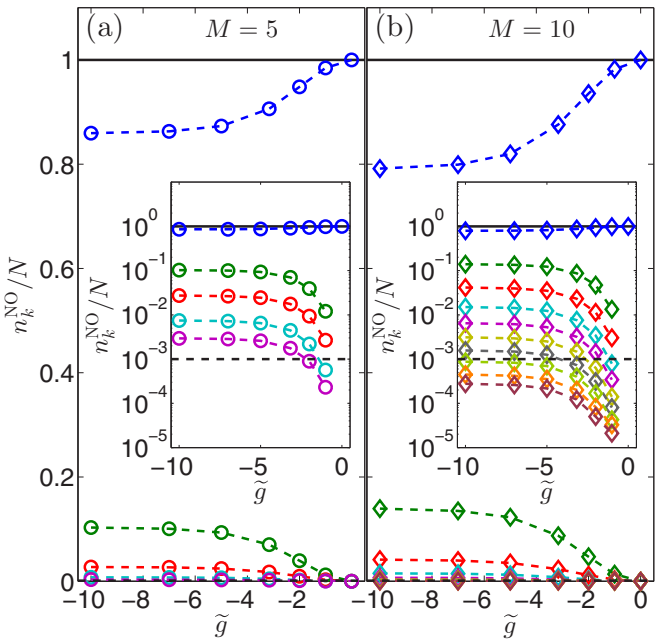

FIG. 6. Natural occupancies n_k^{NO} for the MCTDHB calculations in Fig. 5 for (a) $M = 5$ and (b) $M = 10$. The dashed horizontal line denotes the convergence criterion of $0.1\% = 10^{-3}$ ($N = 2$).

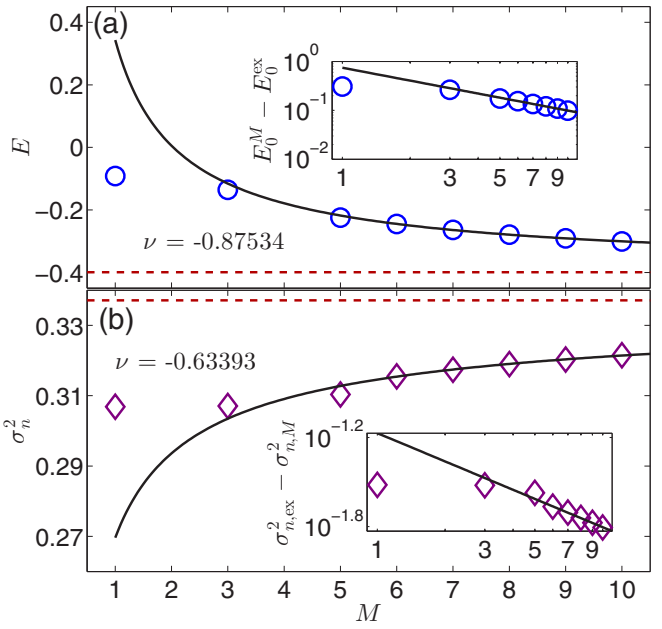

FIG. 7. Convergence with increasing number of modes M for $N = 2$ with $\tilde{g} = -2$: (a) ground-state energy and (b) single-particle density variance. Dashed horizontal lines correspond to exact values. Symbols denote the MCTDHB results for different values of M. The exponent of the power-law fit, ν, is also shown. Inset: Log-log plot of the absolute difference between exact and MCTDHB results.

for strongly attractive interaction and that convergence of the MCTDHB expansion with an increasing number of modes M is exceedingly slow.

In Fig. 6, we present the dependence of the natural occupancy on the interaction parameter. A couple of remarks pointing to the ambiguity of this convergence indicator are in order. First, by looking at the results for $M = 10$ and $\tilde{g} = -10$ one is tempted to conclude that MCTDHB has already converged since three orbitals are below 0.1%. But we know from Fig. 5 that for the same interaction strength the MCTDHB c.m. variance is still far from the exact value. Second, it can be seen that all the natural occupancies, except for the highest one, are shifted up as the number of single-particle modes M is increased. This further exemplifies the failure of the convergence requirement based on the lowest occupancy. For example, the fifth lowest natural occupancy at $\tilde{g} = -2$ is below 0.1% for $M = 5$, while this is not true for $M = 10$, where the fifth single-particle mode is now above the cutoff value.

Finally, we look at the rate of convergence for observables, in particular, the ground-state energy and the single-particle density variance, as depicted in Fig. 7. We find that the MCTDHB results approach the exact values with a slow power law as a function of the number of single-particle modes M, i.e., $|O_{\mathrm{exact}} - O_M| \sim M^{\nu}$. The empirical exponent ν lies between -1 and $-\frac{1}{2}$, which indicates slightly faster convergence than the $-\frac{1}{2}$ leading exponent of the full-configuration-interaction expansion of two one-dimensional bosons with point interaction in a fixed harmonic oscillator basis [46]. We note that this power-law behavior only sets in for mode numbers larger than $M = 6$ in this case and the convergence rate is significantly slower for smaller M. This may be because the variational optimization of the modes is particularly effective for small M. It also means, however, that in the pre-power-law regime of $M < 6$, increasing the number of modes has even less effect than the empirical power law would suggest that governs larger regimes of M. Unfortunately, for particle numbers in the hundreds or larger, the scaling of computational resources practically limits the application of MCTDHB exactly to the small-M regime.

2. Delocalization of the c.m.: Unphysical coupling of c.m. and relative motion

In order to understand how MCTDHB deals with the competing length scales and why it violates the separation of c.m. and relative motion, it is instructive to plot the two-particle density, as shown in Fig. 8 for $N = 2$. In these plots, the diagonal ($x = y$) represents the c.m. coordinate R and the antidiagonal ($x = -y$) the relative motion coordinate r. While Figs. 8(a), 8(c), and 8(e) relate to the ground state of $\tilde{g} = -1$, Figs. 8(b), 8(d), and 8(f) relate to a later time $t\omega_0 = 30$ after trap release. Here the c.m. wave function has expanded significantly according to Eq. (C7), whereas the relative-motion bound state is hardly changed. Figures 8(a) and 8(b) show the exact result and Fig. 8(b) clearly demonstrates the diverging length scales. Note the changing spatial scale between Fig. 8(a) and Fig. 8(b).

Figures 8(c) and 8(d) present the $M = 1$ (Gross-Pitaevskii) result. At this level, the c.m. and relative motion length scales are identical because the product form of the state with a single mode function $|\Psi(x,y)|^2 = |\phi(x)|^2|\phi(y)|^2$ together with the inversion symmetry of the problem forces a fourfold symmetry and leaves no option to distinguish the two diagonal directions.

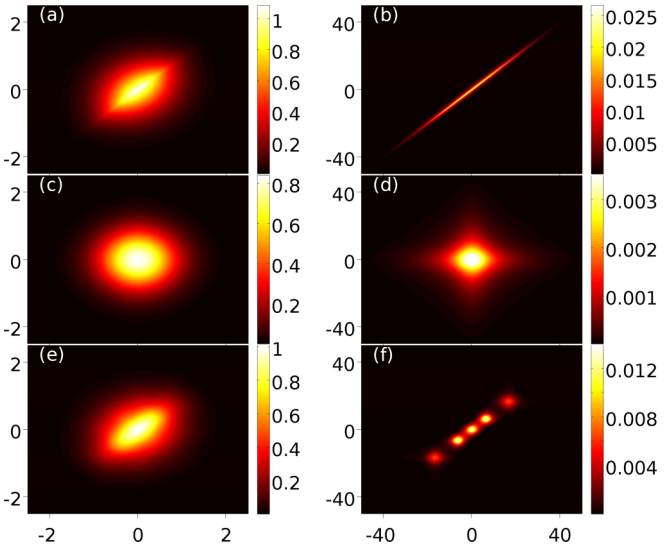

FIG. 8. Two-particle density $\rho^{(2)}(x,y) = 2|\Psi(x,y)|^2$ for $N = 2$ with $\tilde{g} = -1$ at different times: (a, c, e) $t\omega_0 = 0$; (b, d, f) $t\omega_0 = 30$. Comparison between (a, b) exact, (c, d) Gross-Pitaevskii ($M = 1$), and (e, f) $M = 5$.

For long times, the wave function expands in both directions and the c.m. and relative motion length scales are identical.

Figures 8(e) and 8(f) report an MCTDHB simulation with $M = 5$ modes. The trapped ground state in Fig. 8(e) is approximated better than with $M = 1$, although some more detailed features are missing. The long-time profile in Fig. 8(f) shows five separated peaks, with each one exhibiting a fourfold symmetry and resembling the $M = 1$ result, albeit on a different scale. As the MCTDHB expansion is a sum over symmetrized product states, different numbers of modes M will produce up to M peaks with diagonal–off diagonal symmetry. Thus for given M, the c.m. and relative motion are strongly coupled and expansion dynamics, where the c.m. length scale increases over time, will not be captured correctly. Furthermore, this discretized behavior due to finite M leads to an impractical number of M needed to correctly model the limit of a delocalized c.m. but localized relative motion.

APPENDIX E: PROOF OF THE BOUNDS FOR THE WIDTH OF THE SINGLE-PARTICLE DENSITY

In this section, we prove the bounds for the variance of the exact single-particle density manifested in the shaded region in Fig. 4 in the text. For systems with a Hamiltonian that is separable in the c.m. and relative motion coordinate, we can conveniently introduce the change of variables for the c.m. coordinate R,

$$R = \sum_{j=1}^{N} x_j/N, \tag{E1}$$

and for the relative motion coordinate with $i \geqslant 2$ [47],

$$r_i = \sqrt{\frac{i-1}{i}}\left(x_i - \frac{1}{i-1}\sum_{k=1}^{i-1} x_k\right). \tag{E2}$$

This means that the many-body wave function is given by

$$\Psi(x_1,x_2,\ldots,x_N) = \chi(R)\Phi(r_2,r_3,\ldots,r_N). \tag{E3}$$

This allows us to write the single-particle density profile as

$$\rho(x_N) = \int_{-\infty}^{\infty} \prod_{j=1}^{N-1} dx_j F(R) G(r_2,r_3,\ldots,r_N), \tag{E4}$$

where

$$F(R) = |\chi(R)|^2 \tag{E5}$$

and

$$G(r_2,r_3,\ldots,r_N) = |\Phi(r_2,r_3,\ldots,r_N)|^2. \tag{E6}$$

Note that we can express r_N as

$$r_N = \frac{N}{\sqrt{N^2-N}}(x_N - R). \tag{E7}$$

Then we can transform the integration from $\prod_{j=1}^{N-1} dx_j \to |\mathcal{J}| \prod_{j=2}^{N-1} dr_j dR$, where $\mathcal{J}$ is the corresponding Jacobian. The single-particle density becomes

$$\rho(x_N) = |\mathcal{J}| \int_{-\infty}^{\infty} \prod_{j=2}^{N-1} dr_j dR\ F(R) \times G\left(r_2,r_3,\ldots,\frac{N}{\sqrt{N^2-N}}(x_N - R)\right). \tag{E8}$$

The $(N-2)$ integrations over dr_j can now be done separately and be used to define a new function,

$$H(x_N - R) = |\mathcal{J}| \int_{-\infty}^{\infty} \prod_{j=2}^{N-1} dr_j \times G\left(r_2,r_3,\ldots,\frac{N}{\sqrt{N^2-N}}(x_N - R)\right), \tag{E9}$$

which allows us to write the single-particle density as

$$\rho(x_N) = \int_{-\infty}^{\infty} dR\ F(R) H(x_N - R). \tag{E10}$$

One can see that indeed the single-particle density profile is just a convolution between the $|\chi(R)|^2$ and another function H that is associated with the relative motion wave function.

The function H can be further interpreted as the mean density for a fixed COM position. This can be justified by following Ref. [20]. We write the single-particle density in this case as

$$\rho(x'_N|R) = \int_{-\infty}^{\infty} dx_1 \ldots dx_N \delta\left(R - \sum_{k=1}^{N} x_k/N\right) \times \delta(x'_N - x_N)\left|\Phi\left(\frac{x_2 - x_1}{\sqrt{2}}, \sqrt{\frac{2}{3}}\left(x_3 - \frac{1}{2}(x_2 + x_1)\right), \ldots, \times \sqrt{\frac{N-1}{N}}x_N - \sqrt{\frac{1}{N^2-N}}\sum_{k=1}^{N-1} x_k\right)\right|^2. \tag{E11}$$

The integration over dx_N can be easily done due to the presence of the δ function, leading to

$$\rho(x'_N|R) = \int_{-\infty}^{\infty} dx_1 \dots dx_{N-1} \delta\left(R - \sum_{k=1}^{N-1} \frac{x_k + x'_N}{N}\right) \times \left|\Phi\left(\frac{x_2 - x_1}{\sqrt{2}}, \sqrt{\frac{2}{3}}(x_3 - \frac{1}{2}(x_2 + x_1)), \dots, \sqrt{\frac{N-1}{N}} x'_N - \sqrt{\frac{1}{N^2 - N}} \sum_{k=1}^{N-1} x_k\right)\right|^2. \tag{E12}$$

Again we transform the integration variables using Eq. (E2) such that $\prod_{j=1}^{N-1} dx_j \to |\mathcal{J}| \prod_{j=2}^{N} dr_j$, where we define

$$r_N = \sqrt{\frac{N-1}{N}} \left(x'_N - \frac{1}{N-1} \sum_{k=1}^{N-1} x_k\right). \tag{E13}$$

This yields

$$\rho(x'_N|R) = |\mathcal{J}| \int_{-\infty}^{\infty} \prod_{j=2}^{N} dr_j \, |\Phi(r_2, \dots, r_N)|^2 \times \delta\left(R - x'_N - r_N \sqrt{\frac{N-1}{N}}\right). \tag{E14}$$

Finally, we integrate over the dr_N to find that indeed H is equal to $\rho(x_N|R)$:

$$\rho(x'_N|R) = H(x'_N - R). \tag{E15}$$

It is straightforward to show that the variances add in a convolution provided that at least one of the functions is centered at the origin (in our case the c.m. wave function),

$$\sigma_n^2 = \int_{-\infty}^{\infty} (x - \langle x \rangle)^2 (F * H) dx = \sigma_R^2 + \sigma_r^2 \tag{E16}$$

where $\sigma_R^2 = \int_{-\infty}^{\infty} x^2 F(x) dx$, $\sigma_r^2 = \int_{-\infty}^{\infty} (x - \langle x \rangle)^2 H(x) dx$, and the functions F and H are normalized to unity. From Eq. (E16), it can be deduced that the width of the exact single-particle density will always be greater than the width of the c.m. wave function, $\sigma_R^2 \leqslant \sigma_n^2$, and the equality is satisfied in the limit of large interaction $g \to \infty$ ($\sigma_r^2 \to 0$). Moreover, the variance of the relative motion density for a trapped state is smaller than the untrapped case, i.e., $\sigma_r^2 \lessapprox \sigma_{\rm sol}^2$, where $\sigma_{\rm sol}^2$ is an excellent approximation of the untrapped relative motion variance that becomes exact for large N [20]. This means that the bounds for the exact single-particle density must be

$$\sigma_R^2 \leqslant \sigma_n^2 \lessapprox \sigma_R^2 + \sigma_{\rm sol}^2. \tag{E17}$$

[1] I. Bloch, J. Dalibard, and W. Zwerger, Many-body physics with ultracold gases, Rev. Mod. Phys. **80**, 885 (2008).

[2] Q.-Y. He, M. D. Reid, B. Opanchuk, R. Polkinghorne, L. E. C. Rosales-Zárate, and P. D. Drummond, Quantum dynamics in ultracold atomic physics, Frontiers Phys. **7**, 16 (2012).

[3] A. J. Daley, C. Kollath, U. Schollwöck, and G Vidal, Time-dependent density-matrix renormalization-group using adaptive effective Hilbertspaces, J. Stat. Mech. (2004) P04005.

[4] H.-D. Meyer, U. Manthe, and L.S. Cederbaum, The multi-configurational time-dependent Hartree approach, Chem. Phys. Lett. **165**, 73 (1990).

[5] M. H. Beck, A. Jäckle, G. A. Worth, and H.-D. Meyer, The multiconfiguration time-dependent Hartree (MCTDH) method: A highly efficient algorithm for propagating wavepackets, Phys. Rep. **324**, 1 (2000).

[6] J. Caillat, J. Zanghellini, M. Kitzler, O. Koch, W. Kreuzer, and A. Scrinzi, Correlated multielectron systems in strong laser fields: A multiconfiguration time-dependent Hartree-Fock approach, Phys. Rev. A **71**, 012712 (2005).

[7] D. K. Faust and W. P. Reinhardt, Analysis of a Bose-Einstein Condensate Double-Well Atom Interferometer, Phys. Rev. Lett. **105**, 240404 (2010).

[8] O. E. Alon, A. I. Streltsov, and L. S. Cederbaum, Multiconfigurational time-dependent Hartree method for bosons: Many-body dynamics of bosonic systems, Phys. Rev. A **77**, 033613 (2008).

[9] L. Pitaevskii and S. Stringari, *Bose-Einstein Condensation* (Clarendon, Oxford, UK, 2003).

[10] W. Kohn, Cyclotron resonance and de Haas-van Alphen oscillations of an interacting electron gas, Phys. Rev. **123**, 1242 (1961).

[11] G. W. Gibbons and C. N. Pope, Kohn's theorem, Larmor's equivalence principle and the Newton-Hooke group, Ann. Phys. (NY) **326**, 1760 (2011).

[12] L. Khaykovich, F. Schreck, G. Ferrari, T. Bourdel, J. Cubizolles, L. D. Carr, Y. Castin, and C. Salomon, Formation of a matter-wave bright soliton, Science **296**, 1290 (2002).

[13] K. E. Strecker, G. B. Partridge, A. G. Truscott, and R. G. Hulet, Formation and propagation of matter-wave soliton trains, Nature (London) **417**, 150 (2002).

[14] P. Medley, M. A. Minar, N. C. Cizek, D. Berryrieser, and M. A. Kasevich, Evaporative Production of Bright Atomic Solitons, Phys. Rev. Lett. **112**, 060401 (2014).

[15] G. D. McDonald, C. C. N. Kuhn, K. S. Hardman, S. Bennetts, P. J. Everitt, P. A. Altin, J. E. Debs, J. D. Close, and N. P. Robins, Bright Solitonic Matter-Wave Interferometer, Phys. Rev. Lett. **113**, 013002 (2014).

[16] J. H. V. Nguyen, P. Dyke, D. Luo, B. A. Malomed, and R. G. Hulet, Collisions of matter-wave solitons, Nat. Phys. **10**, 918 (2014).

[17] A. L. Marchant, T. P. Billam, M. M. H. Yu, A. Rakonjac, J. L. Helm, J. Polo, C. Weiss, S. A. Gardiner, and S. L. Cornish, Quantum reflection of bright solitary matter waves from a narrow attractive potential, Phys. Rev. A **93**, 021604(R) (2016).

[18] Y. Castin and C. Herzog, Bose-Einstein condensates in symmetry breaking states, C. R. Acad. Sci. Paris Ser. IV **2**, 419 (2001).

[19] J. B. McGuire, Study of exactly soluble one-dimensional N-body problems, J. Math. Phys. **5**, 622 (1964).
[20] F. Calogero and A. Degasperis, Comparison between the exact and Hartree solutions of a one-dimensional many-body problem, Phys. Rev. A **11**, 265 (1975).
[21] A. I. Streltsov, O. E. Alon, and L. S. Cederbaum, Formation and Dynamics of Many-Boson Fragmented States in One-Dimensional Attractive Ultracold Gases, Phys. Rev. Lett. **100**, 130401 (2008).
[22] A. I. Streltsov, O. E. Alon, and L. S. Cederbaum, Scattering of an attractive Bose-Einstein condensate from a barrier: Formation of quantum superposition states, Phys. Rev. A **80**, 043616 (2009).
[23] A. I. Streltsov, O. E. Alon, and L. S. Cederbaum, Swift Loss of Coherence of Soliton Trains in Attractive Bose-Einstein Condensates, Phys. Rev. Lett. **106**, 240401 (2011).
[24] L. Cao, S. Krönke, O. Vendrell, and P. Schmelcher, The multi-layer multi-configuration time-dependent Hartree method for bosons: Theory, implementation, and applications, J. Chem. Phys. **139**, 134103 (2013).
[25] M. Olshanii, Atomic Scattering in the Presence of an External Confinement and a Gas of Impenetrable Bosons, Phys. Rev. Lett. **81**, 938 (1998).
[26] S. Klaiman and O. E. Alon, Variance as a sensitive probe of correlations, Phys. Rev. A **91**, 063613 (2015).
[27] In fact, near zero eigenvalues are not desirable and may create numerical instabilities, since the MCTDHB algorithm relies on inverting the single-particle density matrix [5,8] .
[28] K. Sakmann, A. I. Streltsov, O. E. Alon, and L. S. Cederbaum, Universality of fragmentation in the Schrödinger dynamics of bosonic Josephson junctions, Phys. Rev. A **89**, 023602 (2014).
[29] R. Beinke, S. Klaiman, L. S. Cederbaum, A. I. Streltsov, and O. E. Alon, Many-body tunneling dynamics of Bose-Einstein condensates and vortex states in two spatial dimensions, Phys. Rev. A **92**, 043627 (2015).
[30] S. I. Mistakidis, L. Cao, and P. Schmelcher, Negative-quench-induced excitation dynamics for ultracold bosons in one-dimensional lattices, Phys. Rev. A **91**, 033611 (2015).
[31] J. M. Schurer, A. Negretti, and P. Schmelcher, Capture dynamics of ultracold atoms in the presence of an impurity ion, New J. Phys. **17**, 083024 (2015).
[32] K.-S. Lee and U. R. Fischer, Truncated many-body dynamics of interacting bosons: A variational principle with error monitoring, Int. J. Mod. Phys. B **28**, 1550021 (2014).
[33] U. Manthe, H.-D. Meyer, and L. S. Cederbaum, Wave-packet dynamics within the multiconfiguration Hartree framework: General aspects and application to NOCl, J. Chem. Phys. **97**, 3199 (1992).
[34] A. U. J. Lode, K. Sakmann, O. E. Alon, L. S. Cederbaum, and A. I. Streltsov, Numerically exact quantum dynamics of bosons with time-dependent interactions of harmonic type, Phys. Rev. A **86**, 063606 (2012).
[35] E. H. Lieb and W. Liniger, Exact analysis of an interacting Bose gas. I. The general solution and the ground state, Phys. Rev. **130**, 1605 (1963).
[36] Indeed, the number of terms in the expansion, (2), is given by the binomial coefficient $\binom{N+M-1}{N}$, which changes the scaling from $\sim N$ for $M = 2$ to $\sim c^N$ for $M \approx N$, where c depends weakly on N with $2 \leqslant c \leqslant 2e$.
[37] A. U. J. Lode, A. I. Streltsov, O. E. Alon, H.-D. Meyer, and L. S. Cederbaum, Exact decay and tunneling dynamics of interacting few-boson systems, J. Phys. B **42**, 044018 (2009).
[38] K. Sakmann, A. I. Streltsov, O. E. Alon, and L. S. Cederbaum, Exact Quantum Dynamics of a Bosonic Josephson Junction, Phys. Rev. Lett. **103**, 220601 (2009).
[39] A. U. J. Lode, A. I. Streltsov, K. Sakmann, O. E. Alon, and L. S. Cederbaum, How an interacting many-body system tunnels through a potential barrier to open space, Proc. Natl. Acad. Sci. USA **109**, 13521 (2012).
[40] J. G. Cosme, C. Weiss, and J. Brand (2016) Center-of-mass motion as a sensitive convergence test for variational multi-mode quantum dynamics (supporting data); http://dx.doi.org/10.15128/q237hr938.
[41] T. Ernst and J. Brand, http://github.com/Qiwib/qiwib (2011).
[42] A. I. Streltsov and O. I. Streltsova (2015) MCTDHB—Lab version 1.5; http://mctdhb-lab.com.
[43] T. Busch, B.-G. Englert, K. Rzazewski, and M. Wilkens, Two cold atoms in a harmonic trap, Found. Phys. **28**, 549 (1998).
[44] S. Flügge, *Rechenmethoden der Quantentheorie* (Springer, Berlin, 1990).
[45] R. Schmitz, S. Krönke, L. Cao, and P. Schmelcher, Quantum breathing dynamics of ultracold bosons in one-dimensional harmonic traps: Unraveling the pathway from few- to many-body systems, Phys. Rev. A **88**, 043601 (2013).
[46] T. Grining, M. Tomza, M. Lesiuk, M. Przybytek, M. Musiał, P. Massignan, M. Lewenstein, and R. Moszynski, Many interacting fermions in a one-dimensional harmonic trap: A quantum-chemical treatment, New J. Phys. **17**, 115001 (2015).
[47] X.-J. Liu, H. Hu, and P. D. Drummond, Three attractively interacting fermions in a harmonic trap: Exact solution, ferromagnetism, and high-temperature thermodynamics, Phys. Rev. A **82**, 023619 (2010).